Fluid-solid drag models selection for simulating wheat straw particle movement in anaerobic digester

Yang Yang[1], Hongguang Zhu[1,2*]

(1. *College of Mechanical and Energy Engineering, Tongji University, Shanghai 201804, China*;
2. *Institute of New Rural Development, Tongji University, Shanghai 201804, China*)

Abstract: Computational fluid dynamics (CFD) has been utilized to simulate the movements of wheat straw particles for agitator speed selection in full-scale wet digestion. Previous research has found that the current drag model generally used for depicting the motion of spherical particles cannot match the movement behavior of wheat straw particles with their non-spherical shape. In this study, the sedimentation experiment and horizontal flow experiment of straw particles were determined using a V20-3D camera and a micro Particle Image Velocimetry (PIV) system. With analyses of the experimental data and CFD simulation results, the prediction accuracies of the non-spherical drag models of Hölzer and Sommerfeld (HS), Kishore and Gu (KG), Haider and Levenspiel (HL), Richter and Nikrityuk (RN), and Fabio Dioguardi (FD) were evaluated by the motion of individual straw particles. The results showed that the KG model has a significant advantage over the other drag models, both simulating the particle settling velocities in a one dimensional settling experiment and simulating the predictable trajectory in a two-dimensional horizontal flow experiment. Therefore, the KG drag model was selected to simulate with CFD the wheat straw particle movement to select agitator speeds. Additionally, the realizable k-ε turbulence model was proven to be superior to the other turbulence models for simulating the continuous phase flow with CFD.

Keywords: wheat straw particle, drag model, shape coefficient, image analysis, micro PIV measurement
DOI: 10.25165/j.ijabe.20231602.8003

Citation: Yang Y, Zhu H G. Fluid-solid drag models selection for simulating wheat straw particle movement in anaerobic digester. Int J Agric & Biol Eng, 2023; 16(2): 249–258.

1 Introduction

With the development of clean energy, there has been an increase in the anaerobic digestion of crop straw to produce biogas and hydrogen[1,2]. Under optimal conditions, it is expected that all biomethane will be transferred from the solid-liquid reaction to the gaseous phase, ensuring maximum energy recovery. Due to the high difference in density of solid biomass particles, the separation of a solid-liquid mixture is inevitable[3,4]. Specifically, this is manifested as the sedimentation and floating of straw particles, which is not conducive to fermentation[5,6].

Whether it is gas mixing[7] or mechanical mixing[8], the appropriate mixing of biomass particles needs to be solved to improve anaerobic digestion[9]. Computational fluid dynamics (CFD) simulation technology is a promising technique to study the mixing process between particles and fermentation fluids to optimize the agitator design[10-12] by visualizing the mixing process with simulation.

The simulation method can be single phase simulation or multiphase simulation. In single phase simulation, the mixture of solid particles and fluids is treated as a single phase of non-Newtonian fluids[13,14] Though this method can demonstrate the fluid phase motion, it cannot explain the physical nature of suspension and sedimentation of biomass particles[15]. The method of multiphase simulation can reflect the complex flow behavior in anaerobic reactors by simulating the gas-liquid-solid three-phase flow or solid-liquid two phase flow[15,16].

For the two-phase flow simulation method, the Eulerian-Lagrange method and the Eulerian-Eulerian method were used for simulating the particles and fluid's motion. Which method is selected is based on the volume fraction of the particles. When the volume fraction is less than 20%, the Eulerian-Lagrange method is appropriate to simulate the particle-fluid motion, on the other side, the Eulerian-Eulerian method is better. In the mechanical stirring system of large-scale straw fermentation, in order to maintain better biogas production, large-size straw particles are limited to less than 5% of the volume of the entire fermentation tank[17-19]. However in some large-scale mixed fermentation plants, the large-size particles are less than 20% of the total volume[20]. Treating large-size straw particles as discrete phases, the liquid phase and small particles as fluid phases, ignoring the role of bubbles, and performing CFD calculations with Eulerian-Lagrange two-phase flow meets the assumption of the basic mechanism of sedimentation and suspension of biomass[3,21,22]. The latest experimental studies also support this hypothesis[23].

When calculating the motion of Non-spherical particles while applying the Lagrange discrete phase method, a non-spherical drag model could better describe the moving properties of the biomass particle than a spherical drag model such as the Schiller and Naumann's model[24]. There are some applications of classical non-spherical fluid-solid drag models in the literature.

For example, four drag models have been used to predict the settlement of fly ash in the work of Gerhardter et al.[25] They are the drag model Haider and Levenspiel (HL) with shape coefficient of Ψ[26], drag model Richter and Nikrityuk (RN) with shape coefficient of SR[27] and drag model Kishore and Gu (KG) with shape coefficient of E[28]. The drag model Fabio Dioguardi (FD)[29] was

Received date: 2022-10-28 **Accepted date:** 2023-02-16
Biographies: Yang Yang, PhD candidate, research interest: thermal energy, Email: 1510296@tongji.edu.cn.
***Corresponding author: Hongguang Zhu**, PhD, Professor, research interest: agricultural bioenvironment and energy engineering. College of Mechanical and Energy Engineering, Tongji University, Tel: +86-13764684107, Email: zhuhg@tongji.edu.cn.

used to predict the sedimentation velocity of volcanic ash particles. The drag model of Hölzer and Sommerfeld (HS)[30] was applied to the prediction of lift of non-spherical particles[31].

These non-spherical drag models can be applied to the Eulerian-Lagrange two-phase flow to calculate the sedimentation and suspension process of straw particles.

The translation and rotation of particle motions, is determined by the sedimentation experiment and the horizontal flow experiment of straw particles in water. These experiments were used to evaluate the prediction accuracy of the above five non-spherical drag models on the motion of single discrete phase straw particles. This provides a method to accurately simulate particle movement at varying agitator speeds using the Eulerian-Lagrange model.

2 Material and method

2.1 Drag models of particle-fluid

2.1.1 Relationship between drag coefficient and particle settling velocity

In the wet fermentation biogas project, the volume of wheat straw particle is less than 5% of the volume of biogas tank, thus, the motion of the particles follows the Eulerian-Lagrange approach. The fluid phase was treated as a continuum by solving the Navier-Stokes Equations, while the dispersed phase is solved by tracking a large number of particles, bubbles, or droplets through the calculated flow field. The dispersed phase can exchange momentum, mass, and energy with the fluid phase.

In CFD code, for the continuous fluid phase the mass equation and the momentum equation in the element are Equations (1)-(2) as follows:

$$\frac{\partial\left(\varepsilon_f\rho_f\right)}{\partial \mathrm{t}}+\nabla\cdot\left(\varepsilon_f\rho_f\vec{u}_f\right)=0 \tag{1}$$

$$\frac{\partial\left(\varepsilon_f\rho_f\vec{u}_f\right)}{\partial \mathrm{t}}+\nabla\cdot\left(\varepsilon_f\rho_f\vec{u}_f\vec{u}_f\right)=-\varepsilon_f\nabla p+\nabla\cdot\left(\varepsilon_f\bar{\bar{\tau}}_f\right)+\varepsilon_f\rho_f\vec{g}+R_{f,p} \tag{2}$$

where, ε_f is the volume fraction of fluid phase; ρ_f is the density of the fluid, kg/m^3; $\vec{u}_f$ is the velocity vector of the fluid, m/s, ∇p is the pressure gradient, Pa; $\bar{\bar{\tau}}_f$ is the tensor of stress acting on the fluid element, N/m^2; $\vec{g}$ is the acceleration of gravity, 9.81 m/s^2; $R_{f,p}$ is the force due to the particles acting on the fluid element, N/m^3.

The force of the fluid relative to the particles $R_{f,p}$ is defined by:

$$R_{f,p}=-\frac{F_D}{V_{cell}}=-\frac{m_pF\left(\vec{u}_f-\vec{u}_p\right)}{V_{cell}} \tag{3}$$

For the dispersed phase, the single particle's motion equation is Equation (4) as follows:

$$\frac{d\vec{u}_p}{dt}=F\left(\vec{u}_f-\vec{u}_p\right)+\frac{\vec{g}\left(\rho_p-\rho_f\right)}{\rho_p} \tag{4}$$

where,

$$F=\frac{18\mu_f}{\rho_pd_p^2}\frac{C_DRe_p}{24} \tag{5}$$

$$Re_p=\frac{\rho_f\left|\vec{u}_f-\vec{u}_p\right|d_p}{\mu_f} \tag{6}$$

According to Equations (4)-(6), the velocity of the particle along with time is calculated by Equation (7):

$$\frac{d\vec{u}_p}{dt}=\frac{3}{\rho_pd_p}\frac{C_D}{4}\rho_f\left|\vec{u}_f-\vec{u}_p\right|\left(\vec{u}_f-\vec{u}_p\right)+\frac{\vec{g}\left(\rho_p-\rho_f\right)}{\rho_p} \tag{7}$$

where, $\vec{u}_p$ is the particle velocity, m/s; $\vec{u}_f$ is the fluid velocity, m/s; m_p is the particle mass of the discrete phase, kg; F_D is the force on the particles,[N]; V_{cell} is the calculation domain, m^3; ρ_p is the particle density, kg/m^3; and d_p is the particle diameter, m.

According to Equation (7), the drag coefficient C_D depends on the velocity difference $\vec{u}_f-\vec{u}_p$ and the time t. Specially, in the steady condition, when the fluid is still, the particle velocity is constant, C_D is then only related to the particle settling velocity $\vec{u}_p$.

2.1.2 Drag models for non-spherical particle in the literature

Wheat straw particles are non-spherical particles. The drag coefficient model is related to the particle shape coefficient and particle Reynolds number[32]. In this work, the following five models generally used in the literature are evaluated.

Haider and Levenspiel (HL)[26] studied the drag coefficient C_D and terminal velocity of spherical and non-spherical particles shaped as isometric like cube octahedrons, octahedrons, cubes, tetrahedrons and thin free-falling disks. They derived the equation of drag coefficient C_D related to the particle Reynolds number Re_p and sphericity Ψ, see Equation (8).

$$C_{D,HL}=\frac{24}{Re_p}\left(1+A\cdot Re^B\right)+\frac{C}{\left[1+\frac{D}{Re_p}\right]} \tag{8}$$

where, Ψ is calculated by A_p/A_{sph}, A_p is area of the equal-spherical volume, m^2, $A_{sph}$is the real superficial area of the particle, m^2. $Re_P<2.6\times10^5$,$\Psi>0.67$, A, B, C, D is related to Ψ.

Hölzer and Sommerfeld (HS)[30] proposed a drag model for non-spherical particles (Equation (9)) based on the existing drag models. The drag model $C_D$is based on particle shapes: cube, cube-octahedron, octahedron, tetrahedron, disks and plates, cuboids and cylinders.

$$C_{D,HS}=\frac{8}{Re}\frac{1}{\sqrt{\Psi_{\parallel}}}+\frac{16}{Re}\frac{1}{\sqrt{\Psi}}+\frac{3}{\sqrt{Re}}\frac{1}{\Psi^{3/4}}+0.42\cdot10^{0.4(-\log\Psi)^{0.2}}\frac{1}{\Psi_{\perp}} \tag{9}$$

where, $Re_p<1\times10^4$.$\Psi_{\perp}=\frac{1/4\pi d_v^2}{A_p}$, $\Psi_{\parallel}=\frac{1/4\pi d_v^2}{1/2A_{sph}-A_p}$. $\Psi_{\parallel}$is the lengthwise sphericity, the $\Psi_{\perp}$ is crosswise sphericity.$1/4\pi d_v^2$ is the area of the equal-spherical volume, m^2; A_{sph} is the real area of the particle, m^2; A_p the projected cross-sectional area of the particle perpendicular to the flow, m^2.

Kishore and Gu (KG)[28] proposed a drag model based on ellipsoidal particles (Equation (10)), where, E is the aspect ratio in two dimensions, L and B are the length and width of the particle, m. The range of E is $0.25\le E\le2.5$.

$$C_{D,KG}=\frac{24\cdot E^{0.49}}{Re_p}(1.05+0.152Re_p{}^{0.687}E^{0.671}) \tag{10}$$

Richter and Nikrityuk (RN)[28] developed a drag model shown as Equation (11), which based on spherical, ellipsoidal and cubic particles, shape coefficient $SR=l_p/d_v$, l_p is the particle length parallel in the flow direction, m; d_v is the diameter of an equivalent-volume sphere, m. The range of Reynold number is $10\le Re_P\le250$.

$$C_{D,RN}=0.21+\frac{20}{Re_p}SR^{0.58}+\frac{6.9}{\sqrt{Re_p}}SR^{-1.4} \tag{11}$$

Fabio Dioguardi (FD)[29] studied the pumice particles' drag model related to particle Reynold number Re_p and shape factors Φ.$\Phi=\Psi/X_p$, $X_p=P_p/P_{mp}$, where X_p is a circularity, P_p is perimeter of projection area, m; P_{mp} is perimeter of projection area of an equal-spherical volume, m. The range of Re_P is defined by $1\le Re_P\le10^5$.

$$C_{D,FD}=\frac{0.9627}{Re^{0.079}\Phi^{1.6}} \tag{12}$$

2.2 Geometric shape and density of straw particles

The wheat straw was obtained from Funan County, Anhui Province, China. Two kinds of treated wheat straw particles were selected to do the test. One was cut into pieces, called sheared particles, as shown in Figure 1a. The other type of particle used was rubbed by a screw machine, named rubbed particles, as shown in Figure 1b.

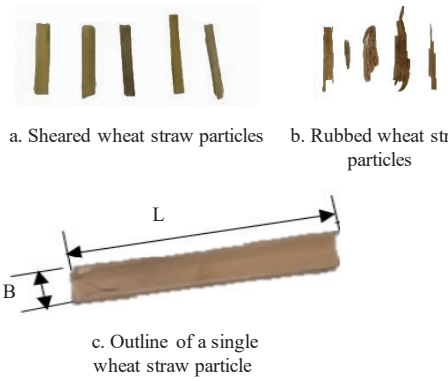

a. Sheared wheat straw particles b. Rubbed wheat straw particles

c. Outline of a single wheat straw particle

Figure 1 Geometric appearance for two kinds of straw particles

The particle shapes are measured as follows. Firstly, all the particles were wetted by water, 24 sheared particles and 134 rubbed particles were picked randomly. Then the images of each particle were captured by a camera. Finally, the geometries for both kinds of straw particles were calculated by comparing the image resolution with the real size of the particle. the geometry and the outline of both types of particles are presented in Figure 1c. L is the length of particle's maximum projection (m), and B is the width (m). The maximum projection was calculated from the images. The length of both types was less than 10 mm, the width varied from 1 mm to 6 mm. The particle mass m_P was measured by a precision balance with range of 0-120 g and an accuracy of ±1 mg.

The density of the two kinds of particles fell in a small range. To calculate the density of rubbed particles conveniently, the mean density was used since it was easier to get the density of a single particle. The density of the particle ρ_p and the density of water ρ_f were measured by a standard Gay–Lussac pycnometer with the volume of 100 mL. The volume of a particle V_p is calculated by the ratio of m_p/ρ_p. And the particle equivalent thickness T is also calculated by the ratio of V_p/A_{pmax}.

2.3 Drag model evaluation by one dimensional settling experiment

According to Equation (7), when the water is still, the particle velocity will be constant, the existing drag models were evaluated by comparing the settling velocities of experiments with simulations.

2.3.1 Settling velocity

The free-settling experiment was conducted in a square tank made of acrylic glass, as shown in Figure 2a.

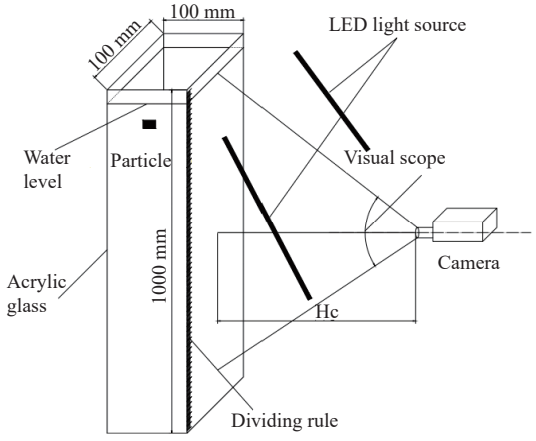

a. Diagram of the experimental setup

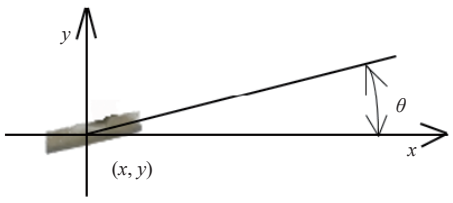

b. Particle centroid position and angle θ between the length axis and horizontal plane

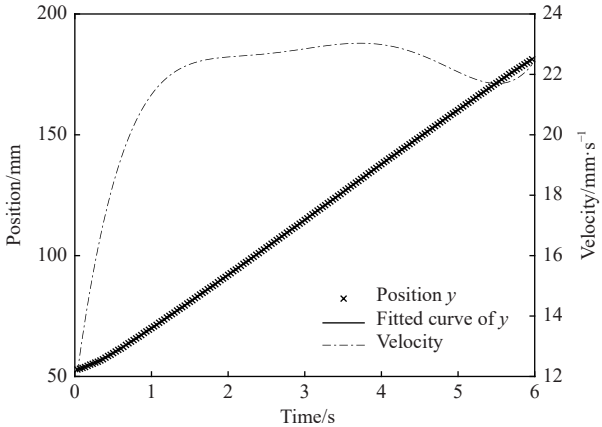

c. Position and velocity of wheat straw particle change with time

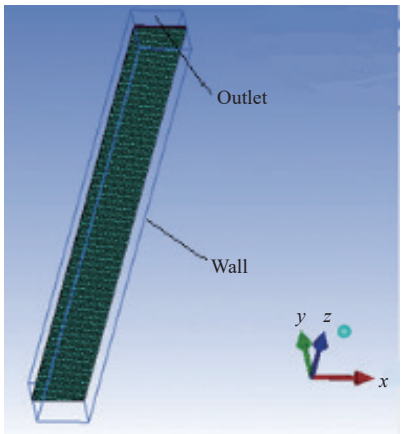

d. Mesh of cubic tube for simulating the particle settling

Figure 2 Setup of particle settling velocities measurement

The experimental water tank is transparent and its length, width, height and thickness are 100 mm, 100 mm, 1 m and 5 mm, respectively, as shown in Figure 2a. A white paper is placed on one side of the tank, and a V20-3D camera is positioned on the opposite side facing the paper. The frame rate of the camera is 30 fps and its resolution is 1080×1920 pixels. A LED light source with 120 W was used to illuminate the region of interest in the tank. A millimeter-scale ruler is attached to the left side of the water tank and used to assess the falling position of the particles. The distance between the camera and the water tank is denoted as Hc. The camera focus was adjusted to ensure that the ruler could be clearly captured. The height of the camera's visual scope is 500 mm.

In the experiment, a camera will record the particle's drop from the top to the bottom of the vessel. The particles are added slowly to the tank one by one. The video records the whole process, and the videos are converted into photographs frame by frame using Photoshop software. Then 30 pictures in PNG format are produced per second using MATLAB software.

Based on the data from the images, some parameters are calculated. They are the centroid y coordinate and the orientation angle θ[33] of the particle in every image, as shown in Figure 2b. the terminal settling velocity $u_{experiment}$ and the relationship of y vs t, as shown in Figure 2c.

2.3.2 Numerical simulation setup

ANSYS Fluent 17.0 was used to do the numerical simulation of the particle falling in the still water. The settling velocities are acquired by tracking the discrete particle motion. The geometry and mesh of the container for simulation is shown in Figure 2d. A hexahedral structure mesh for square tubes was used. The maximum mesh length is 5 mm and the Hexahedral non-structural mesh is used. Mesh quality is, so mesh independency is not needed to be discussed. The single-phase coupling method is adopted to calculate the particle phase.

2.3.3 Drag model evaluation

According to Equation (7), when the velocity of fluid is constant, the relative error between the experiment velocity and simulation velocity can be determined to evaluate the existing drag models, which is calculated by Equation (13).

$$\text{relative error} = \frac{\left|\mathrm{u}_{simulation} - \mathrm{u}_{experiment}\right|}{\left|\mathrm{u}_{experiment}\right|} \quad (13)$$

2.4 Drag models' evaluation by a two-dimensional flow experiment

According to Equation (7), when the velocity of fluid is not constant, the particle-fluid drag coefficient is related both to the difference of fluid velocity and the particle velocity, and time. According to multiphase flow theory of Particle Motion Theory, a turbulence model should be selected for continuous phase flow calculation first. After the fluid velocity field calculation, the particle trajectory, particle velocity and particle runtime can be calculated.

2.4.1 Turbulence model selection

The accurate fluid velocity simulation comes from applying a reliable turbulence model, which is generally confirmed by PIV measurement[34,35]. ANASYS Fluent gives a series of turbulence models to model the momentum transfer equation. The best turbulence model will then be selected.

a) PIV measurement

The PIV measurement experiment was carried out in a water tank with horizontal flow, the schematic of the experiment is presented in Figure 3a. The length, width, height, and thickness of the tank are 300 mm, 100 mm, 205 mm and 5 mm, respectively. The inlet and outlet of the water tank are 30 mm, as seen in Figure 3b. Before the experiment, the horizontal flow rate in the tank should be adjusted to a suitable level to meet the range of the flow field of the actual straw anaerobic digester. This experiment employed a micro-PIV system (ILA, Germany) to measure the local velocity field with the experimental setup shown in Figure 3a. The water flow rate at the inlet of the tank is set at 350 L/h. The fluid velocity distribution at the y=0 plane (Figure 3b) is measured through the system. Figure 3d shows the PIV velocimetry area with a size of 50 mm×140 mm. The images are processed for the velocity vectors with the PIVVIEW demo software (Daheng Galaxy Viewer (x64)).

b) Continuous phase simulation

Before the continuous phase simulation, boundary conditions and mesh of the geometry should be set. The boundaries of the water tank are inlet, outlet, wall and Up. Zone Up is a free surface next to air (Figure 3c). The inlet velocity is set to 0.2263 m/s, water density and viscosity are set up with the default settlings. A hexahedral structure mesh is used for the water tank, where the maximum length is 5 mm, the number of mesh is 1 192 808, and the mesh quality is 0.4. The particle diameter is less than 0.5 mm, so then the scale of the mesh is suitable.

In the horizontal flow experiment, the flow Reynolds number at the entrance of the tank is 5630, and the flow is turbulent. ANSYS Fluent supports many turbulence models to calculate the momentum Equation (10). Considering the economy and rationality of calculations, the vortex motion of turbulence, the low Reynolds number characteristics of the flow region, RNG k-ε model, low-re k-ε turbulence model, realizable k-ε model and SST-kw model were evaluated. The velocity field is obtained from the region of PIV measurement zone in order to pick the best turbulence model by comparing it with the velocity distribution.

2.4.2 Particle trajectory

a) Particle trajectory acquisition by experiment

When the flow rate is stable, a single straw particle is released as shown in Figure 3f. The particle motion trajectory will be recorded by the camera in Figure 3e. Due to the low velocity flow of the water inlet, a V20-3D camera with 30 fps is used. The particle position changes with time and the particle position will be extracted by image analysis.

b) Particle trajectory acquisition by simulation

Since the volume of the particle is far less than the whole volume of the container, and the particle motion does not influence fluid flow condition, one way coupling is used to do the simulation. Particle properties are added into the discrete phase setup, and five drag models were coded in the UDF function for particle trajectory tracking allowing particle position information canto be acquired.

2.4.3 Drag models' evaluation

According to Equation (7), the particle trajectory or particle velocity, and particle runtime can be the evaluation criteria for the drag models. Because the particle trajectory reflects the state of the particle moving down for sedimentation and/or suspension, particle

Table 1 Wheat straw particle parameters used in the horizontal experiment

m_p(kg)	V_p(m³)	L(m)	B(m)	T(m)	A_{pmax}(m²)	dv(m)	Ψ	Φ	$\Psi_{\parallel}$	$\Psi_{\perp}$	SR	E
0.014	13.33	10.58	3.03	0.55	18.9	2.94	0.34	0.25	0.11	0.36	0.61	3.49

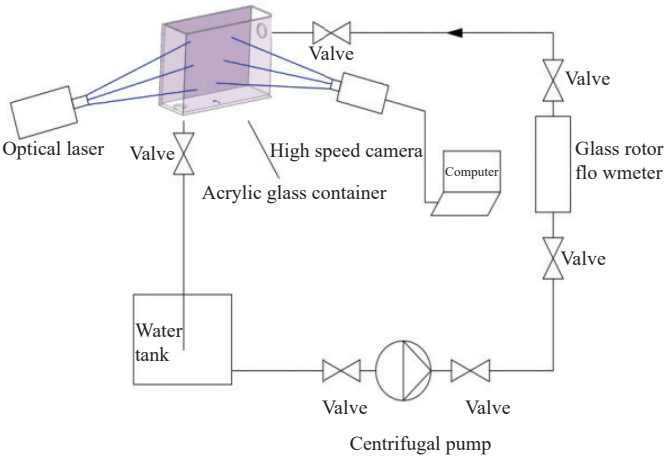

a. Diagram of flow velocity measurement by micro-PIVsystem

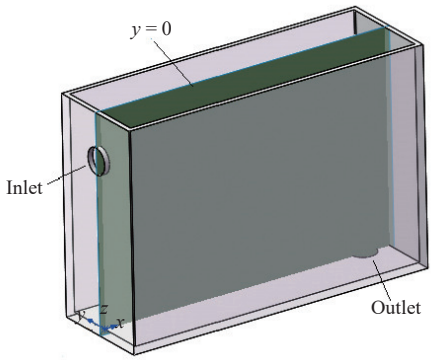

b. Geometry plane of PIV plane for flow field measurement

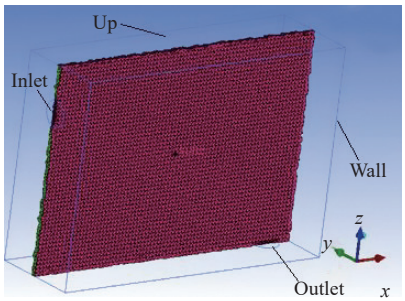

c. Mesh of geometry plane for simulation

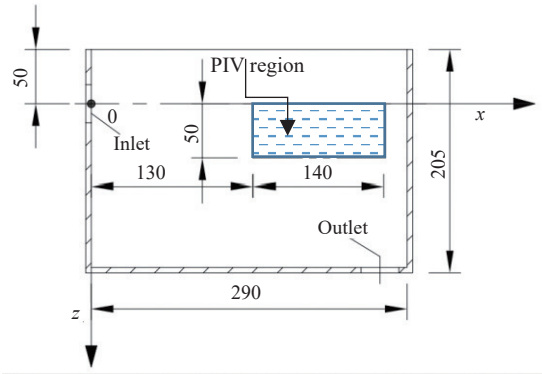

d. PIV measurement plane

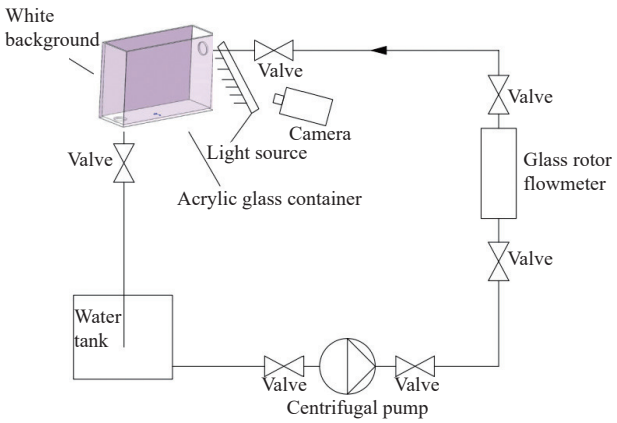

e. Particle trajectory measurement setup

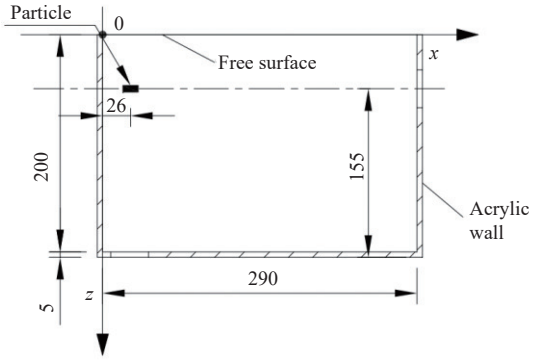

f. Particle release position in $y = 0$ plane

Figure 3 PIV measurement for turbulence model selection and particle motion measurement in two-dimensional horizontal flow

trajectory and runtime are obtained by both experiment and simulation.

The timing starts as the particle moves close to the boundary of the water tank, and then when it changes downward the time is recorded. In other words, the time is evaluated while the particle is moving in the horizontal flow.

After that, the distance error between the measured value and the simulated value during the movement process is calculated. Therefore, the cumulative error between simulation data and experiment data can be calculated by Equation (14).

$$\text{Culmulative error} = \sum_{t=t_0}^{t=t_n} \sqrt{(X1(t)-X(t))^2+(Z1(t)-Z(t))^2} \quad (14)$$

where, $X1(t)$ and $Z1(t)$ are the simulation particle displacement with drag model, $X(t)$ and $Z(t)$ are particle displacement by experiments. t_0 and t_n are times that obtained by experiments or simulations.

3 Results and discussion

3.1 Particle geometry parameters and settling velocities

3.1.1 Particle geometry parameters

The measurement of the length, width, and height of sheared particles and rubbed particles are listed in Figure 4. The range of length, width and height are 9.5-11 mm, 1-5 mm, 0.2-0.5 mm for sheared particles, respectively and 5-30 mm, 1-4 mm, 0.1-1.5 mm for rubbed particles, respectively. Then the particle shape coefficient is calculated by particle geometry. Figure 4c describes particle size distribution of actual digesters for both shear particles and rubbed particles. Particle distributions in these digesters comes

from work of Hans-Joachim et al.[20] In the digester, almost 80% of the biomass particles are less than 1 mm in volume such that they move easier within the water. The particle size distribution is in the range of 1-2 mm, 2-3 mm, 3-4 mm and those greater than 4 mm are less than 10 mm. The particle size in the experiment are larger than 1 mm (Figure 4c).

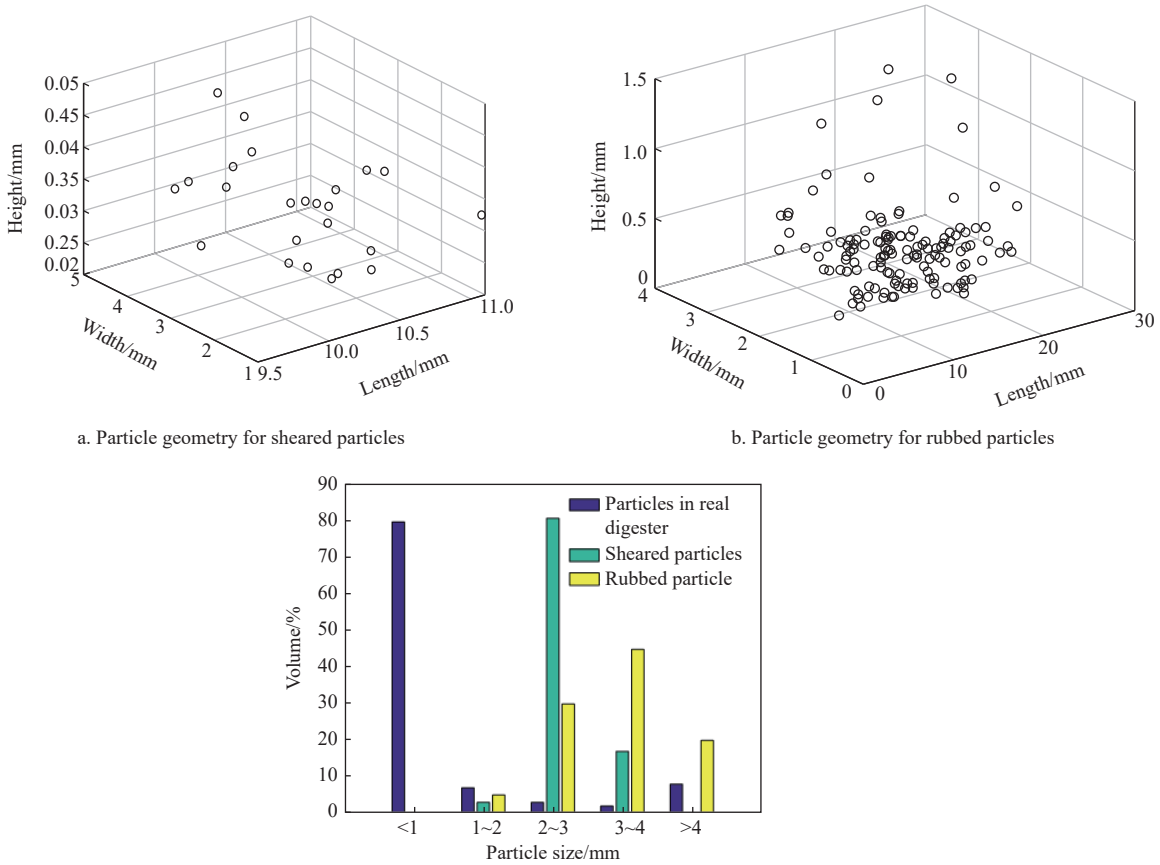

a. Particle geometry for sheared particles

b. Particle geometry for rubbed particles

c. Particles size distributions comparison of the real digester, the sheared particles and the rubbed particles

Figure 4 Particle geometry and size distribution for shear particles and rubbed particles

3.1.2 Settling velocity

Figure 5 depicts the settling velocity relationship with the number of sheared wheat straw particles and rubbed particles during the test. The result indicated that the settling velocity of sheared particles is in the range of 0.014-0.023 m/s (Figure 5a), and the rubbed particles is in the range of 0.005-0.04 m/s (Figure 5b). The results further revealed the dispersion settling velocity distribution in the sheared particles while the intensive settling velocity distribution in the rubbed particles. It might be related to the total number of the selected sheared particles, which is less than the total number of the selected rubbed particles.

3.2 Drag models comparison by one dimensional settling experiment

3.2.1 Prediction error of the drag models for simulating the settling velocity of particles in experiment

Settling velocities obtained by simulation using drag models of HS, KG, HL, RN and FD are depicted in Figure 6.

Through CFD simulation, the settling velocity of 24 shear particles and 134 rubbed particles using the drag models; HS, KG, HL, RN and FD and the relative errors are determined and plotted in

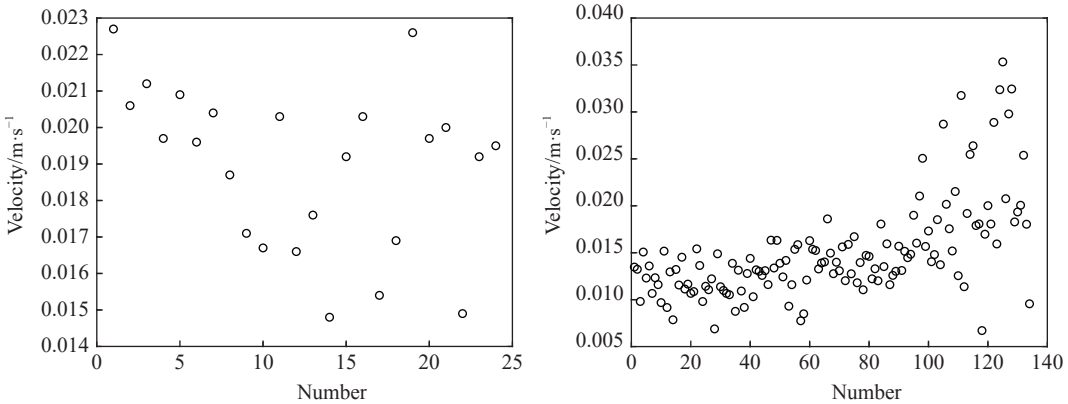

a. Settling velocity of sheared particles

b. Settling velocity of rubbed particles

Figure 5 Settling velocity of particles obtained by experiment

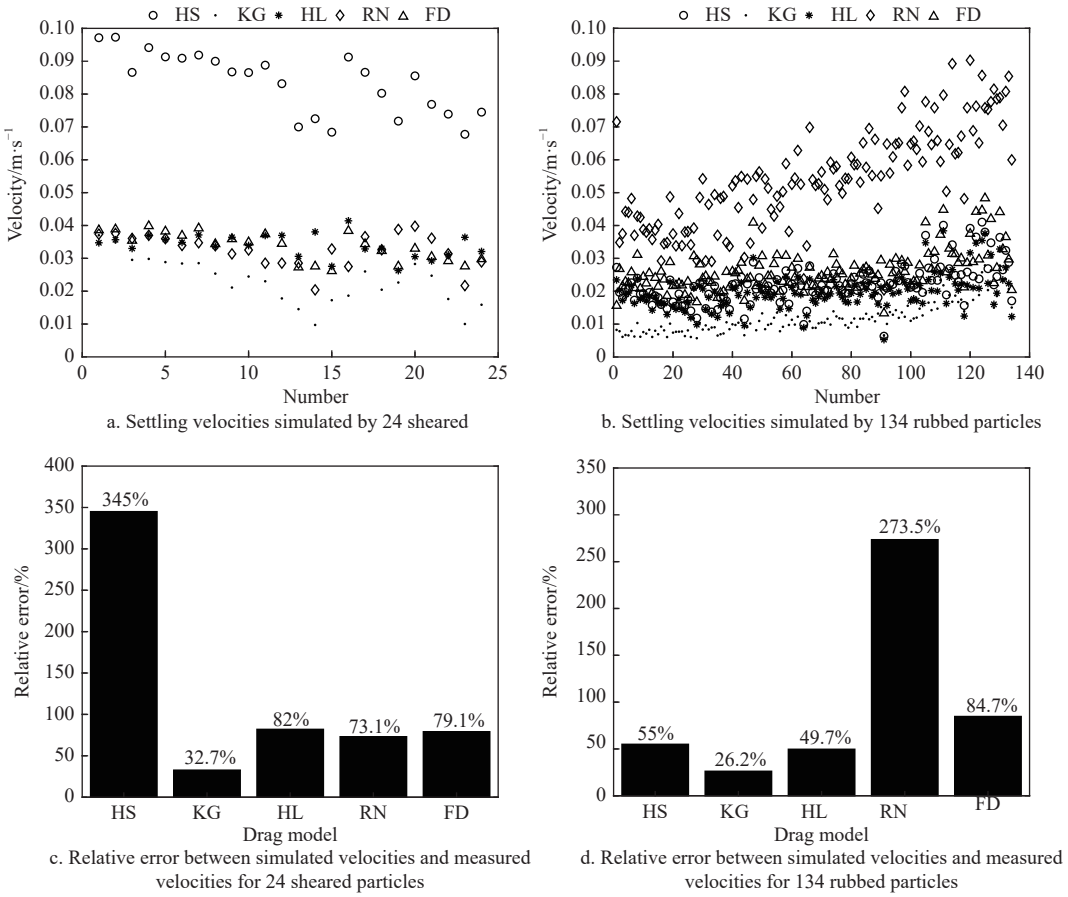

a. Settling velocities simulated by 24 sheared particles

b. Settling velocities simulated by 134 rubbed particles

c. Relative error between simulated velocities and measured velocities for 24 sheared particles

d. Relative error between simulated velocities and measured velocities for 134 rubbed particles

Figure 6 Settling velocities by CFD simulation and relative error between simulated velocities and measured velocities using drag models of HS, KG, HL, RN and FD

Figure 6. Figure 6a shows that KG model has the smallest error, the HS model has the largest error, and Figure 6d indicates that the KG model also has the smallest error, but here the RN model has the largest error.

By making a comprehensive comparison of the relative error among the five different drag models described in Figure 6, it can be seen that the KG model has the smallest error compared to the other drag models in the particle settling experiment. The values of relative error are 32.7% for sheared particles and 25.2% for rubbed particles, with an average error of 28.9% for the two types of particles.

3.2.2 Comparison with simulation error in literatures

Comparison with the result in the literature, the prediction error is not the smallest between measured data and simulation data for particles moving in a fluid. For example, the mean prediction error is 28.9% in the present study, which is far less than the 50% in the work of Gerhardter et al.[25], and is approximate to the 22% in the work of FD[31]. However, the result is inferior to 14.1%-17.7%, 6.7%-21.7%, ±4% and 3.6%-6.0% in the work of FD[29], HS[30], HL[26], KG[28] and RN[27], respectively. The particles used in the first two studies were actual engineering powder particles with extremely irregular shapes. The research object was slag in the work of Gerhardter et al., and volcanic ash was analyzed in the work of FD. Both slag and volcanic ash complex shapes are not artificially controllable. However, the particles used in the last four studies are artificial engineering powder particles and have manmade isometric geometry. The shapes of particles studied were sphere, isometric particles, cuboids, cylinders, disks and plates in the work of HS, cube octahedrons, octahedrons, cubes and tetrahedron in the work of HL, spheroids in the work of KG, and cube and axially symmetric ellipsoids in the work of RN. Therefore, for actual engineering particles such as straw particles, the KG model in this study has potential for engineering applications with a competitive prediction errors to similar studies.

3.3 Drag models' evaluation by two-dimensional horizontal flow experiment

3.3.1 Turbulence model selection

Through PIV measurement the velocity distribution of the PIV region (Figure 4d) is acquired as shown in Figure 7a. Velocity in the y=0 plane is also acquired by CFD simulation using the five different drag models. Because the particles move along with the water flow, the main flow velocity will be important for the in describing the motion of the particles.

The velocity contours and pathlines simulated by the realizable k-ε turbulence model described in Figures 7a and 7b agree with the experiment phenomena. The simulation results show that along the inlet direction, the flow rate of the water gradually decreases, and two streams of fluid are formed approaching the wall surface. One stream flows into the Up surface and the other flows downward which then forms a chaotic flow. The circulating flow inside the container can affect the measurement result. Thus, the velocity region in the horizontal line from inlet to the wall will be compared (Figure 7c).

According to Figure7c, in the line of $z=-5$ mm, velocity fluctuated in the range of 0.1-0.15 m/s along the x coordinate., When x is larger than 0.24 m, the velocity decreases as the water flow rate decreases rapidly when it reaches the wall area. The velocity simulated by the turbulence models of RNG k-ε, low-re k-ε, realizable k-ε, and SST-kw are compared with the PIV velocity shown in Figure 7d. The velocity obtained by the turbulence model

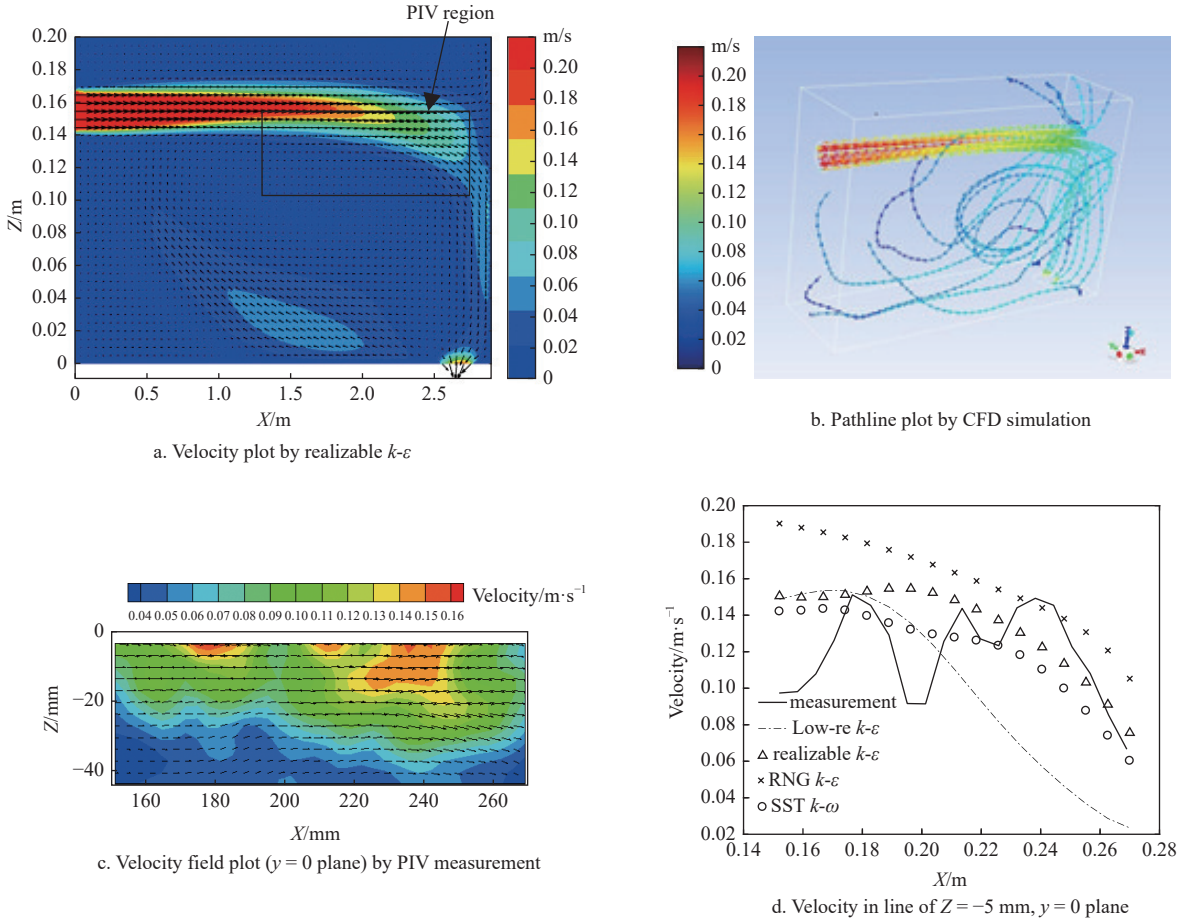

a. Velocity plot by realizable *k-ε*

b. Pathline plot by CFD simulation

c. Velocity field plot (y = 0 plane) by PIV measurement

d. Velocity in line of Z = −5 mm, y = 0 plane

Figure 7 Turbulence model selection by PIV measurement in the PIV region

of realizable *k-ε* has the closest trend compared to the PIV measurement. Therefore, the realizable *k-ε* turbulence model is used in this study for continuous phase calculation for two-dimensional simulation.

3.3.2 Drag models' comparison by particle trajectories and runtimes

After calculation of the continuous phase flow field using the realizable k-ε turbulence model, particle trajectories are acquired for the 5 drag models. In Figure 8a, the particle moves along with the horizontal water flow, when approaching the boundary of water tank, the particle moves downward along with the water flow. There is a specific point where the particle changes path at the end of the horizontal flow. The runtime of the path between the start point and the end point is depicted in Figure 8a.

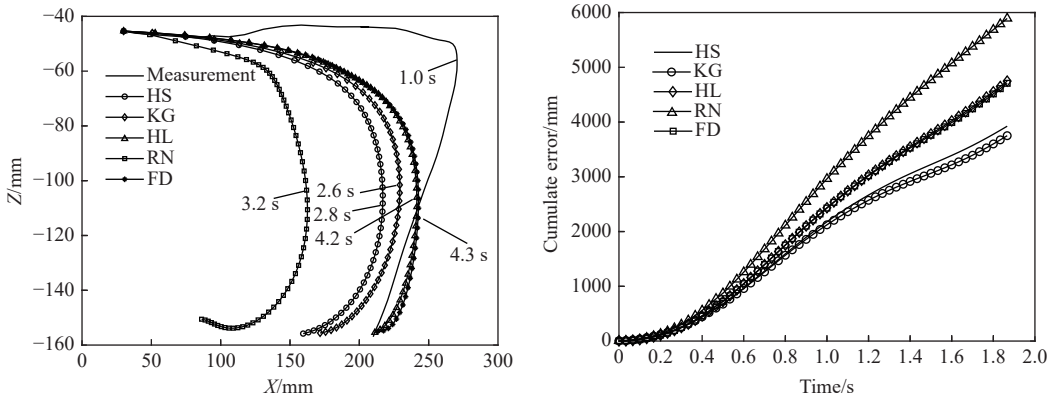

a. Particle trajectories from drag models'prediction andexperiment at different times

b. Cumulative error between simulation and experiment by the 5 drag models

Figure 8 Particle trajectories from drag models' prediction and experiment and cumulative error between simulation and experiment by the 5 drag models

The runtimes of trajectories for the drag models of HS, KG, HL, RN, and FD are 2.8 s, 2.6 s, 4.2 s, 3.2 s and 4.4 s, respectively. The experiment runtime is 0.97 s. Initially, the trajectories of HL and FD are closer to the real particle trajectory. But the runtime of KG is closer to the real particle runtime.

By Equation (14), cumulative errors between simulation and experiment by the 5 drag models are obtained, see Figure 8b. KG model has the least cumulative error than the others.

In a summary, KG model presents the best performance among the five drag models in the two-dimensional horizontal flow

experiment.

3.4 Comprehensive evaluation for the five drag models

3.4.1 Comparison for prediction accuracy

The drag model of KG has the advantage over the other drag models in simulating the particle motion in the one dimensional settling experiment and the two-dimensional horizontal flow experiment.

There are some reasons to explain why the KG drag model is best. Firstly, the functional relationship of KG model can be clearly divided into pressure term and drag term, which follows the principle of fluid drag on particles. Secondly, the shape coefficient of aspect ratio E can better reflect the particles' actual shapes.

Though the drag model provides a good prediction for the particle settling velocity, the cumulate error is a large length (more than 3000 mm). Moreover, a precise drag model should be further developed to satisfy particle motion in two dimensions (2D) or 3D conditions.

3.4.2 Discussion of the science of the experiments

In the study of multiphase flow, continuous phase is the basic phase of fluid, mixing or agitation act directly on the continuous phase, and the movement of the dispersed phase is the result of mechanical interaction between continuous phase and dispersed phase. Therefore, the common continuous phase setup is not suitable for anaerobic digestion mixing process (like CSTR or USR) CFD calculation. Direct agitation is rarely used in the experiment of motion model development, since the three-dimensional data are not stable, these effects on agitation are relatively complex. However, most of the motion models in the existing literature adopt simple one-dimensional precipitation or two-dimensional horizontal motion for development. This study also absorbed classical research methods to develop a straw particle resistance model, rather than directly placing it in the three-dimensional agitation experiment. In addition, the movement of straw particles is the main mass transfer process in straw fermentation. Therefore, the development of a drag model for straw particles is of great significance for the precise design of large-scale anaerobic fermentation stirring systems using straw as raw material.

4 Conclusions

To improve the reliability of CFD using Eulerian-Lagrange two-phase flow method for agitation design of an anaerobic digester, fluid-solid drag models selection for simulating wheat straw particle movement in anaerobic digesters are investigated in this study. Conclusions are drawn as follows:

(1) This study conducted an one-dimensional settling experiment and two-dimensional horizontal flow experiment by using five drag models. It is hypothesized that these take large-size straw particles into consideration as discrete phases and take the liquid phase and small particles as fluid phases. It is shown that the KG model has the minimum prediction error compared to other drag models of HS, HL, RN and FD.

(2) Based on both the settling and two-dimensional horizontal flow experiments, using the non-spherical drag models with the Eulerian–Lagrange method, the KG model can also predict the particles settling velocity and can be used as the non-spherical drag model to simulate the motion of wheat straw particles in water for further biogas project design.

The movement of straw particles is the main mass transfer process in straw fermentation. The development of the drag model for straw particles is of great significance for the precise design of large-scale anaerobic fermentation stirring systems using straw as raw material. Comparison of the simulation and experiment with drag models, resulted in indicating that combined non-spherical drag models with the Eulerian-Lagrange method can commendably predict the particle suspension and settlement.

Acknowledgements

This research was financially supported by the key technology and demonstration project (2018YFC1903204) of the Ministry of Science and Technology of China.

[References]

[1] Huo L L, Yao Z L, Jia J X, Zhao L X, Cong H B, Meng H B, et al. Evaluation of different clean heat supply modes based on crop straws in the rural area of Northern China. Int J Agric & Biol Eng, 2020; 13(5): 209–217.

[2] Zhang Z P, Zhang Q G, Yue J Z, Li L H, Zhang T, Liu Z B. CFD modeling and experiment of heat transfer in a tubular photo-bioreactor for photo-fermentation bio-hydrogen production. Int J Agric & Biol Eng, 2017; 10(1): 209–217.

[3] Tong H, Zhou B Y, Liu C M, Wachemo A C, Li X J, Zuo X Y. Improving biomethane yield by strengthening acidification of maize stover in two-phase anaerobic digestion. Int J Agric & Biol Eng, 2020; 13(4): 226–231.

[4] Chi Y, Wang Y, Li M F, Ren J, Chi Y J. Numerical simulation and experimental study on eggshell membrane separation device. Int J Agric & Biol Eng, 2019; 12(2): 173–183.

[5] Das T, Usher S P, Batstone D J, Rees C A, Stickland A D, Eshtiaghi N. Shear and solid-liquid separation behaviour of anaerobic digested sludge across a broad range of solids concentrations. Water Research, 2022; 222: 118903.

[6] Luo J, Meng H B, Yao Z L, Wachemo A C, Yuan H R, Zhang L, et al. Anaerobic co-digestion of sodium hydroxide pretreated sugarcane leaves with pig manure and dairy manure. Int J Agric & Biol Eng, 2018; 11(4): 224–229.

[7] Annas S, Elfering M L, Jantzen H A, Scholz J, Janoske U. Experimental analysis of mixing-processes in biogas plants. Chemical Engineering Science, 2022; 258: 117767.

[8] Neuner T, Meister M, Pillei M, Koch M, Rauch W. Numerical and experimental flow investigation using ultrasonic PIV for optimizing mechanically agitated lab-scale anaerobic digesters. Chemical Engineering Science, 2022; 264: 118–129.

[9] Cui Y Y, Zhang H B, Li X W, Yang M J, Guan Z L. Computational and experimental investigation of laminar flow mixing system in a pitched-blade turbine stirred tank. Int J Agric & Biol Eng, 2018; 11(4): 111–117.

[10] Leonzio G. Study of mixing systems and geometric configurations for anaerobic digesters using CFD analysis. Renewable Energy, 2018; 123: 578–589.

[11] Wang J, Xue Q W, Guo T, Mei Z L, Long E S, Wen Q, et al. A review on CFD simulating method for biogas fermentation material fluid. Renewable and Sustainable Energy Reviews, 2018; 97: 64–73.

[12] Zhang Y, Yu G R, Siddhu M A H, Masroor A, Ali M F, Abdeltawab A A, et al. Effect of impeller on sinking and floating behavior of suspending particle materials in stirred tank: A computational fluid dynamics and factorial design study. Advanced Powder Technology, 2017; 28(4): 1159–1169.

[13] Li L L, Wang K, Wei L L, Zhao Q L, Zhou H M, Jiang J Q. CFD simulation and performance evaluation of gas mixing during high solids anaerobic digestion of food waste. Biochemical Engineering Journal, 2022; 178: 108279.

[14] Li J, Suvarna M, Li L Y, Pan L J, Pérez-Ramírez J, Ok S Y, Wang X N. A review of computational modeling techniques for wet waste valorization: Research trends and future perspectives. Journal of Cleaner Production, 2022; 367: 133025.

[15] Yu L, Ma J W, Frear C, Zhao Q B, Dillon R, Li X J, Chen S L. Multiphase modeling of settling and suspension in anaerobic digester. Applied Energy, 2013; 111: 28–39.

[16] Trad Z, Vial C, Fontaine J P, Larroche C. Mixing and liquid-to-gas mass transfer under digester operating conditions. Chemical Engineering Science, 2017; 170: 606–627.

[17] Das T, Usher S P, Batstone D J, Rees A C, Stickland D A. Nicky Eshtiaghi. Shear and solid-liquid separation behaviour of anaerobic digested sludge

across a broad range of solids concentrations. Water Research, 2022; 222: 118903.

[18] Yang Y, Zhu H G. Clustering and modelling of rheological parameters for anaerobic digestion materials (ADMs) and its application for feed pump selection. IOP Conference Series:Earth and Environmental Science, 2020; 467: 012053.

[19] Guo H G, Li Q, Wang L L, Chen Q L, Hu H W, Cheng D J, et al. Semi-solid state promotes the methane production during anaerobic co-digestion of chicken manure with corn straw comparison to wet and high-solid state. Journal of Environmental Management, 2022; 316: 115264.

[20] Naegele H, Mönch-Tegeder M, Haag N L, Oechsner H. Effect of substrate pretreatment on particle size distribution in a full-scale research biogas plant. Bioresource Technology, 2014; 172: 396–402.

[21] Rezavand M, Winkler D, Sapp J, Seiler L, Meister M, Rauch W. A fully Lagrange computational model for the integration of mixing and biochemical reactions in anaerobic digestion. Computers & Fluids, 2019; 181: 224–235.

[22] Sheikh A H, Savari C, Barigou M. A data-driven stochastic model for velocity field and phase distribution in stirred particle-liquid suspensions. Powder Technology, 2022; 411: 117940.

[23] Danican A, Darrehmane A, Chateau T, Trad Z, Fontaine J P, Vial C. Development of a multiparticle optical trajectography technique for hydrodynamic analysis of a stirred tank devoted to dark fermentation, Chemical Engineering Journal, 2022; 453: 139521. doi: 10.1016/j.cej. 2022.139521.

[24] Schiller L, Naumann A. A drag coefficient correlation. Zeitschrift des Vereins Deutscher Ingenieure, 1935; 77: 318–320.

[25] Gerhardter H, Prieler R, Mayr B, Knoll M, Mühlböck M, Tomazic P, et al. Evaluation of drag models for particles and powders with non-uniform size and shape. Powder Technology, 2018; 330: 152–163.

[26] Haider A, Levenspiel O. Drag coefficient and terminal velocity of spherical and nonspherical particles, Powder Technol, 1989; 58: 63-70.

[27] Richter A, Nikrityuk A P. Drag forces and heat transfer coefficients for spherical, cuboidal and ellipsoidal. particles in cross flow at sub-critical Reynolds numbers. International Journal of Heat and Mass Transfer, 2012; 55: 1343–1354.

[28] Kishore N, Gu S. Momentum and heat transfer phenomena of spheroid particles at moderate Reynolds and Prandtl numbers, Int. J. Heat Mass Transf, 2011; 54: 2595–2601.

[29] Dioguardi F, Dellino P, Mele D. Integration of a new shape-dependent particle–fluid drag coefficient law in the multiphase Eulerian–Lagrange code MFIX-DEM. Powder Technology, 2014; 260: 68–77.

[30] Hölzer A, Sommerfeld M. New simple correlation formula for the drag coefficient of non-spherical particles. Powder Technology, 2008; 184: 361–365.

[31] Mema I, Mahajan V V, Fitzgerald W B, Padding T J. Effect of lift force and hydrodynamic torque on fluidisation of non-spherical particles. Chemical Engineering Science, 2019; 195: 642–656.

[32] Nikku M, Jalali P, Ritvanen J, Hyppänen T. Characterization method of average gas–solid drag for regular and irregular particle groups. Powder Technology, 2014; 253: 284–294.

[33] Carranza F, Zhang Y. Study of drag and orientation of regular particles using stereo vision, Schlieren photography and digital image processing, Powder Technol, 2017; 311: 185–199.

[34] Hu Y Y, W J, Poncin S, Cao Z P, Li Z H, Li Z H. Flow field investigation of high solid anaerobic digestion by Particle Image Velocimetry (PIV). Science of the Total Environment, 2018; 626: 592–602.

[35] Dapelo D, Alberini F, Bridgeman J. Euler-Lagrange CFD modelling of unconfined gas mixing in anaerobic digestion. Water Research, 2015; 85: 497–511.